EUROPEAN FUSION DEVELOPMENT AGREEMENT

EFDA–JET–PR(03)53

H. Weisen, A. Zabolotsky, X.Garbet, D. Mazon, L. Zabeo, H. Leggate,
M. Valovic, K.-D.Zastrow and JET EFDA contributors

Shear Dependence of Density Peaking in JET

Shear Dependence of Density Peaking in JET

H. Weisen[1], A. Zabolotsky[1], X.Garbet[2], D. Mazon[2], L. Zabeo[2], H. Leggate[3], M. Valovic[3], K.-D.Zastrow[3] and JET EFDA contributors*

[1]Centre de Recherches en Physique des Plasmas Association EURATOM-Confédération Suisse École Polytechnique Fédérale de Lausanne CH-1015 Lausanne,Switzerland
[2]Association EURATOM-CEA, Cadarache, F-13108 St. Paul-lez-Durance, France
[3]EURATOM/UKAEA Fusion Association, Culham Science Centre, Abingdon, OX14 3DB, UK
** See annex of J. Pamela et al, "Overview of Recent JET Results and Future Perspectives", Fusion Energy 2000 (Proc. 18th Int. Conf. Sorrento, 2000), IAEA, Vienna (2001).*

Preprint of Paper to be submitted for publication in
Plasma Physics and Controlled Fusion

ABSTRACT.
Density peaking in source-free L-mode plasmas with Lower Hybrid Curren Drive (LHCD) is observed to increase with increasing peaking of the current profile. For the discharges investigated, the relationship can be summarised as $n_{e0}/\langle n_e \rangle \cong 1.2 l_i$, where l_i is the normalised internal inductance. These observations are strongly supportive of theories explaining particle convection by the Curvature Pinch or Turbulent Equipartition. They were made in a series of MHD-quiescent LHCD plasmas, including positive and negative central magnetic shear, as well as fully current driven plasmas with negligible Ware pinch and no core particle source. No evidence was found of an Anomalous Thermodiffusive contribution to the convective flux. ELMy H-modes, although NBI fuelled, have a qualitatively similar dependence of density peaking on shear.

1. INTRODUCTION

The nature of the inward particle pinch, which leads to the observed peaking of the density profile in tokamaks and stellarators, has been subject to controversy for some time. Recent experiments of fully current driven plasmas with negligible particle source in Tore Supra [1] and TCV [2],[3] have shown that substantial peaking is obtained in the absence of the Ware pinch ($V_{Ware} \propto E_{tor}/B_{pol}$). Transport simulations for a variety of JET discharges have also concluded that an anomalous pinch must be present in the gradient zone ($r/a>0.5$), at least in L-mode plasmas [4]. The main theoretical candidates for explaining this level of convection are Turbulent EquiPartition (TEP) [5],[6] or equivalently, it's fluid counterpart, the Anomalous Curvature Pinch [7], Anomalous ThermoDiffusion [7][8][9] and possibly Neoclassical Thermodiffusion [10] in regions with reduced anomalous particle diffusivity.

A substantial database modelling analysis of density peaking in Ohmic and ECH plasmas in TCV [2], which was constituted mainly of Ohmically relaxed, sawtoothing discharges, did not allow to determine which of TEP or Anomalous Thermodiffusion was the major contributor, because in these discharges the overall shear (or current profile peaking) remained correlated with the degree of peaking of the electron temperature profile, as well as with the sawtooth inversion radius, all of which scale with current profile peaking parameter $\langle j \rangle /(j_0 q_0)$, where $\langle j \rangle = I_p/A$ is the cross-sectional average toroidal current density, $j_0 q_0 = 2(1+\kappa_0^2)B_0/(\mu_0 \kappa_0 R_0)$, j_0, q_0, κ_0, B_0 and R_0 are the axial current density, safety factor, elongation, toroidal field and major radius [11][12]. The parameter $\langle j \rangle /(j_0 q_0)$ is the generalisation to arbitrary plasma shape of the historical scaling parameter $1/q_a$, which describes profile peaking in sawoothing tokamak discharges with circular cross section [13]. Since in sawtoothing plasmas q_0 is approximately unity, we hypothesised that rather $\langle j \rangle / j_0$ than $\langle j \rangle /(j_0 q_0)$ would be the more general scaling parameter. For a given plasma shape $\langle j \rangle / j_0$ is proportional to q_0/q_{95}.

The sawtooth-free Lower Hybrid Current Driven (LHCD) JET L-mode discharges, described in the following, produced a range of current profiles for a fixed value of $\langle j \rangle /(j_0 q_0)$, which are very different from those accessible in sawtoothing regimes, ranging from normal shear to substantially reversed shear. They allow us test the above hypothesis and to check wether or not TEP predictions

are verified at negative shear. A scan of q_{95} performed in a series of normal shear sawtoothing ELMy H-modes shows that density peaking is dependent on overall shear in H-modes as well.

2. DENSITY PEAKING IN SOURCE-FREE L-MODES

The data for this study were obtained from a series of Lower Hybrid Current Driven (LHCD) L-mode discharges in JET, with LHCD powers in the range 0 (Ohmic) to 3.65MW, part of which were produced to demonstrate safety factor profile control using the JET real time control system [14]. Full current drive with $V_{loop} \cong 0$ was obtained at the highest powers available, as shown in the example of fig.1, for otherwise similar discharges with $q_{95} \cong 8$ and $0.8\times10^{19}\,\mathrm{m}^{-3} \le \langle n_e \rangle \le 1.4\times10^{19}\,\mathrm{m}^{-3}$. LHCD drives an off-axis current, thereby broadening the current profile and for sufficient power, producing a hollow current profile [14]. This range of LH powers allowed the creation of a variety of magnetic shear profiles, ranging from normal at low power to strongly reversed at the highest power levels. Examples of the corresponding safety factor profiles are shown in fig.2 and were obtained by EFIT equilibrium reconstructions, which used Faraday rotation data from the JET interfero-polarimeter as constraints [16]. Some of the discharges also had a small amount (<5MW) of centrally deposited ICRH heating. Despite having reversed shear profiles, these plasmas did not produce internal transport barriers, presumably because of the lack of centrally deposited auxiliary power. Electron temperature and density profiles from LIDAR Thomson Scattering (LTS), normalised to the central values, are shown in figs.3 and 4 and appear to be little or not affected by the differences in shear. The profiles shown are averaged over 1 second in stationary conditions in order to improve the rather poor signal-to-noise ratio of the LTS diagnostic at these low densities, for which uncertainties on individual data points are some 20%.

The continuity equation for the particle density $n = n_{e,i}$ can be expressed as $\frac{\partial n}{\partial t} = -\nabla(Vn - D\nabla n) + S$, where $-D\nabla n$ and ∇n are diffusive and convective fluxes respectively and S is the particle source. Both the diffusive and the convective fluxes may be of neoclassical or of anomalous origin, although anomalous fluxes are generally much larger. Since no neutral beam injection was used in these plasmas, the only particle source is due to edge fuelling. The penetration of neutrals from the edge was calculated using the Kn1D code [17]. By radially integrating the above particle source, the source term $\Gamma_s(r) = \int_a^r S dr'$ can directly be compared to the flux terms, as shown in fig.5 (solid line). Since particle fuelling is localised to the outer 10% of the cross section, it is immediately apparent that the particle source cannot explain the observed density gradients.

The fact that the absolute value of the flux is not known is unimportant as long as we are only interested in profile shapes. This allows us to undertake the following Gedanken experiment: We assume that there is no convection and that the source term has to balance the diffusive flux. Realistic profiles for D, used to model particle and impurity transport in wide variety of situations, range from quadratic in minor radius, as assumed in fig.5, to flat (see e.g. [18]). We see that, if the diffusive flux is assumed to be balanced in steady state by the source term near the plasma edge, this cannot, by a large margin, be the case in the bulk of the discharge. In fig.5 (broken lines) we

have estimated the diffusive flux by assuming D=1m^2/s at the edge, a value typical for particle transport experiments [18]. (The exact value is not important for the above argument). If the diffusivity profile were flat, the discrepancy would be larger still. Hence in the bulk of the discharge the density profile in steady state must result from a balance of diffusion and convection, such that $\nabla n/n = V/D$. The fact that the density profiles remain peaked for $V_{loop} \cong 0$ also shows that a pinch mechanism other than the Ware pinch must be responsible.

In order to search for systematic dependencies, the data from these experiments were used to assemble a profile database of some 100 timeslices in quasi-stationary conditions with constant $\langle j \rangle / (j_0 q_0)$. Despite averaging the data over 1 second to reduce statistical noise, LTS profiles remained too noisy to serve as a reliable indicator of density profile peaking. Instead, we used a peaking factor $n_{e0}/\langle n_e \rangle$, where $\langle ... \rangle$ is a volume average, derived from Far Infrared Interferometry on JET, using an Abel inversion based on the shape of the magnetic flux surfaces. This definition of peaking factor (or profile width), corresponds, for monotonic profiles, to values between 0 and 1.

Figure 6 shows, as expected for TEP, that for constant $\langle j \rangle / (j_0 q_0)$, density peaking depends on overall shear expressed as $\langle j \rangle / j_0$ in normal shear plasmas defined by $q_{min} = q_0$. The relationship can be expressed approximately as $\langle n_e \rangle / \langle n_{e0} \rangle \approx 0.25 + 1.67 \langle j \rangle / j_0$. The symbol types in the figure refer to electron temperature peaking $\langle T_e \rangle / T_{e0}$ from LTS, showing, that within the range of variation of this parameter, no dependence is discernible in the dataset. In fig.7 we have plotted $\langle n_e \rangle / \langle n_{e0} \rangle$ as a function of a qualitative indicator of temperature peaking determined from electron cyclotron emission, confirming that there is no correlation with temperature peaking. This indicator was chosen as the normalised temperature difference between the core and a point at 60% of the minor radius. (ECE data beyond some 65% of the minor radius were overwhelmed by downshifted radiation from LHCD generated suprathermal electrons). The symbols in fig.7 are for classes of $\langle j \rangle / j_0$, showing that there is no correlation between $\langle j \rangle / j_0$ and $\langle T_e \rangle / T_{e0}$, which would allow the results to be interpreted either by TEP or Thermodiffusion.

When reversed shear discharges are included in the analysis, $\langle j \rangle / j_0$ ceases to be a suitable scaling parameter, fig. 8, as already expected from the observation that the density profiles are insensitive to shear reversal (fig.4). The various symbols in fig.8 refer to classes of q_{min}/q_0 as determined using the real time polarimeter inversion routines of the JET real time control system JET [19]. $\langle n_e \rangle / \langle n_{e0} \rangle$ correlates however fairly well with q_{min}/q_{95} (not shown), irrespective of shear. The best data alignement is obtained with the internal inductance, l_i, which can be determined independently from the equilibrium reconstruction. As a filter for data quality, the present dataset was restricted to reconstructions which yielded values for l_i, which up a systematic deviation (0.1), were consistent with the evaluation based only on the corresponding Shafranov integral. In order to conserve the appearance of fig.7 and for consistency with ref.[2], we have plotted $\langle n_e \rangle / \langle n_{e0} \rangle$ versus $1/l_i$ in fig.9. We are not aware of an a priori theoretical reason for the good correlation $\langle n_e \rangle / \langle n_{e0} \rangle \approx 0.83/l_i$ with this particular measure of current profile peakedness.

Since the Abel inversion may in principle be prone to systematic errors, we cross checked this

dependence using a qualitative but sensitive measure of peaking based on the ratio of the line average densities from a central and an off-axis interferometer chord. This is only admissible for a dataset with the same plasma geometry as is the case here. Both chords are nearly horizontal, making them also insensitive to possible changes in core geometry caused by small differences in the Shafranov shift. The result in fig.10 shows that the chord ratio follows $1/l_i$ in the same way as the peaking factor derived from the Abel inversion. This figure is also resolved into classes of average electron density, showing that the absolute density, which determines the depth of neutral penetration, has no effect on the peakedness of the density profile.

The following figures show that, once the dependence on l_i is acknowleged, the loop voltage (fig.11) and the LHCD power (fig.12) have no further influence, although both are of course correlated with l_i . Similarly, the addition of central RF power up to 4.9MW did not lead to any noticeable changes in density peaking. chord ratio

3. MODELLING OF DENSITY PROFILES

We first modelled these density profiles semi-empirically by assuming a pinch velocity $V = -\eta D \nabla q/q$, as in ref.[2]. Since the peaking is insensitive to the loop voltage and to electron temperature gradients, neither the Ware pinch, nor thermodiffusion are considered here. The modelled peaking is in reasonable agreement for normal shear if $\eta \sim 0.4$, but fails to describe reversed shear plasmas, for which it predicts hollow density profiles, which are clearly outside the error bars of the LTS diagnostic. More generally however, the predictions for TEP include both a shear term and a term arising from the finite aspect ratio, the latter of which always produces peaking. A model based on an approximate formula for 'canonical' profiles, proposed by Isichenko [5] and Garbet [7] for plasmas with circular cross section,

$$n(r) \approx n_0 \left\{ -1 \frac{4}{3R_0} \int_0^r \left(\frac{d \ln q}{d \ln r} + \frac{3}{8} \right) d\ln r' \right\}$$

is in good agreement with the data (fig.13), and doesn't produce hollow profiles even in the cases with the strongest shear reversal. The above expression was evaluated by replacing r with the volume coordinate $\sqrt{V/V_{tot}}a$ and using safety factor profiles from polarimeter constrained equilibrium reconstructions. The number of datapoints is smaller than in the previous figures because good reconstructions were only obtained for a subset of the data. Figure 14 shows examples of model profiles produced using the above expression and the safety factor profiles shown in fig.2.

Although there is good agreement of TEP/curvature pinch predictions with positive shear, we must be aware that this should not necessarily be expected at low or negative shear. Anomalous pinches exist as a result of microturbulence caused by TEM and ITG modes. If these modes are suppressed or stabilised, as may be the case at low or negative shear, the corresponding pinches would be absent too. In the discharges described here, this would still leave neoclassical pinches other than the Ware pinch, such as neoclassical thermodiffusion for which $\nabla T_{e,\,neo} = D_{neo} \nabla T_e (2T_e)$

in axisymmetrical geometry [10]. In the absence of any other convective mechanism and anomalous diffusion, this pinch tends to produce density profiles such that $\nabla n_e / n_e = \nabla T_e / (2T_e)$. Another neoclassical effect may be the pinch arising from the presence of the fast electrons carrying the off-axis LH driven current, which would tend to broaden the density profile. Inspection of Fig.12, which shows that the same density peaking can be obtained for Ohmic and high power LHCD plasmas for nearly the same values of l_i (around $1/l_i \sim 0.9$ on the figure), suggests however that this contribution cannot be significant

4. COMPARISON WITH DENSITY PROFILES IN H-MODE

It is instructive to compare the above source-free, MHD-quiescent discharges with NBI heated sawtoothing, ELMy H-modes with different values of q_{95}, such as the pulse shown in fig.15. In these case q_0 is close to unity and the peaking of the current profile $\langle j \rangle / j_0 \propto q_0 / q_{95}$ for a fixed boundary shape depends only on q_{95}. Both during the L-mode phase and during the ELMy H-mode the density profile is moderately peaked. This density peaking is insensitive to the plasma collisionality and density, except at the highest densities, where the peaking can be stronger than for the discharges shown here [20]. ELM-free H-modes, on the other hand are characterised by flat or slightly hollow density profiles and a rapidly rising average density. Figures 16 and 17 show the electron temperature and density profiles, normalised to their central values, as measured by LTS in the ELMy phases of three discharges with different plasma currents and q_{95}. For the discharge in fig.15, a density profile obtained during the ELM-free H-mode immediately following the H-mode transition, is also shown (broken line). Individual profiles during the ELMy phase exhibit substantial scatter, presumably depending on timing during the ELM cycle, which is why the profiles shown were averaged over the duration of the ELMy phases (several seconds). The figures show that both the temperature and the time-averaged density profiles broaden as q_{95} decreases ($\langle j \rangle / j_0$ increases). The average density peaking factor $\langle n_e \rangle / n_{e0}$, observed in the ELMy phase is in the range 0.7-0.9 for q_{95} ranging from 4.3 to 2.9, albeit for broader current profiles than the L-modes described above, since $\langle j \rangle / j_0$ was in the range 0.35-0.5.

This behaviour is qualitatively consistent with the L-mode observations reported above and with the interpretation of density peaking being due to TEP. In this case however other transport processes contribute to shaping the density profile to an unknown extend. Therefore these observations, unlike the quiescent L-modes presented above, could not be used to make a compelling claim for TEP, or indeed any of the other mechanisms, being the dominant one. These H-mode plasmas have a central particle source from the neutral heating beams and a finite loop voltage, making central fuelling and the Ware pinch probable contributors. Sawteeth regularly flatten the central part of the density profile, whilst large ELMs, by expelling particles from the region just inside the pedestal, transiently increase the peaking. The influence of these factors is itself dependent on q_{95}: The loop voltage, the sawtooth inversion radius, the average ELM period and amplitude decrease as q_{95} increases. Since the presence of sawteeth and ELMs makes these discharges non-

stationary, an assessment of the relative importance of the various processes in H-modes would require the usage of diagnostics and transport simulations with high time resolution. Recent simulations of JET H-modes using the JETTO transport code ascribe density peaking in H-modes in roughly equal parts to the Ware pinch and to an anomalous pinch [4].

CONCLUSIONS

The degre of peaking of the density profiles in source-free L-mode plasmas in JET is in agreement with predictions from anomalous transport theories for TEP (kinetic picture) respectively the Curvature Pinch (fluid picture). The peaking of the density profiles scales with the peaking of the current profiles, expressed as $n_{e0}/\langle n_e \rangle \approx 1.2 l_i$, for the plasma shapes of this experiment. For normal shear plasmas, this relation can also be expressed as $\langle n_e \rangle / (n_{e0}) \approx 0.25 + 1.67\ \langle j \rangle / j_0$ in the range investigated ($0.22 \leq \langle j \rangle / j_0 \leq 0.34$). There is no experimental evidence in this set of experiments, for peaking due to Anomalous Thermodiffusion. A contribution from the Ware pinch can be exluded for the fully current driven plasmas in the dataset. Unlike previous observations of the anomalous pinch [1-3], the present LHCD experiments have clearly identified TEP as the dominant anomalous process of particle convection at normal shear. The density profiles are in fair agreement with the canonical profiles proposed by Isichenko [5] and Garbet [7], even in regions with reversed shear. These theories predict a scaling with l_i which is very similar to the experimentally observed one. In the shear reversed central part the above-mentioned theories predict flat, but not hollow profiles, even for the most reversed shear profiles in the dataset. The central part of the experimental profiles is somewhat more peaked than the canonical profiles, especially at reversed shear. Granting that the theory, in the form included in the model, remains applicable near the axis, this suggests that an additional peaking mechanism may have to be invoked in the plasma core. A plausible candidate is Neoclassical Thermodiffusion, if anomalous transport in the core is low enough, as would have to be established by a comprehensive transport modelling approach. Density peaking in ELMy H-modes has a similar dependence on magnetic shear, although processes other than anomalous pinches contribute to shaping the ELMy H-mode density profiles.

ACKNOWLEGMENTS.

The support of the entire JET-EFDA operating and diagnostics teams is gratefully acknowledged. We wish to thank B. Labombard for generously making the Kn1D code available. This work was partly supported by the Swiss National Science Fund.

REFERENCES

[1]. G.T.Hoang, C.Bourdelle, B.Pégourié, B.Schunke et al, Phys. Rev. Lett. **90** (2003)155002

[2]. A.Zabolotsky, H.Weisen, TCV Team,Plasma Phys. Control. Fusion **45** (2003)735

[3]. I. Furno, H. Weisen, TCV Team, Physics of Plasmas **10** (2003) 2422

[4]. L.Garzotti et al.'Particle transport and density profile analysis in different JET plasmas ' accepted for publication in Nuclear Fusion (2003/2004)

[5]. M.B.Isichenko, A.V.Gruzinov, P.H.Diamond and P.N.Yushmanov, Phys. Plasmas 3 (1996)1916
[6]. D.R.Baker et al.,Nuclear Fusion **40** (2000)1003
[7]. X.Gar et et al.,Physical Review Letters **91** (2003)03500
[8]. J.Weiland 'Collective modes in inhomogeneous plasmas 'IOP Publishing Ltd, 2000, Bristol & Philadelphia, ISBN 0 7503 0589 4 hbk
[9]. F.Jenko F.,Phys. Plasma **7** (2000)514
[10]. L. M. Kovrizhnykh, Nucl. Fusion **24**, (1984) 851
[11]. H.Weisen et al, Physics of Plasmas **6** (1999)1
[12]. H.Weisen et al, Nucl. Fusion **42** (2002)136
[13]. V.Arunasalam et al., Nuclear Fusion **30** (1990)2111
[14]. D.Mazon et al, Plasma Phys. Control. Fusion **45** (2003)L47
[15]. A.Ekedahl et al, Nucl. Fusion **38** (1998)1397
[16]. G.Braithwaite et al, Rev. of Scient. Instrum **60**, 2825
[17]. B.La om ard (MIT), PSFC Research Report **PSFC-RR-01-03** (2001) http://www.psfc.mit.edu/library/01RR/01RR003/01RR003_full.pdf
[18]. The JET Team, Nucl. Fusion **39** (1999)1891
[19]. L.Zabeo et al., Plasma Phys. Control. Fusion **44** (2002)2483
[20]. M.Valovic et al, 30th Fusion St.Petersburg (2003) P-1.105

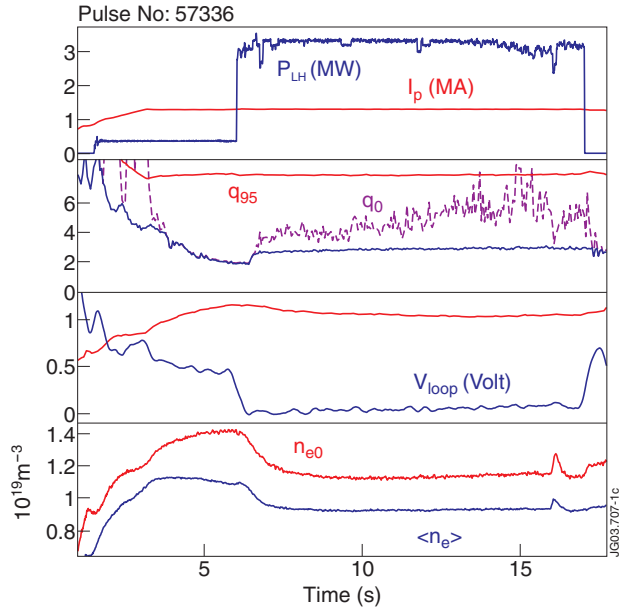

Figure 1: Evolution of a JET LHCD discharge with $V_{loop} \cong 0$. Top pane:time dependence of plasma current and LH power. Second pane: q_{95}, axial safety factor and minimum of safety factor profile from polarimetry. Third pane: Internal inductance and toroidal loop voltage Bottom pane: Axial and average electron densities from interferometry

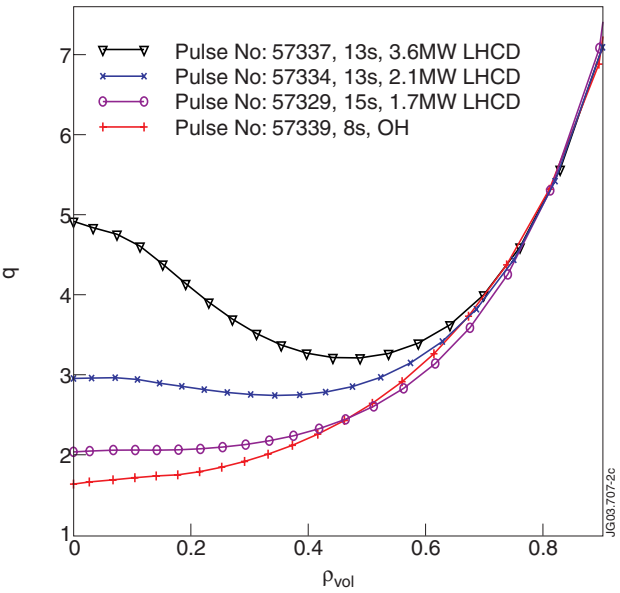

Figure 2: Safety factor profiles obtained with differents levels of LHCD.

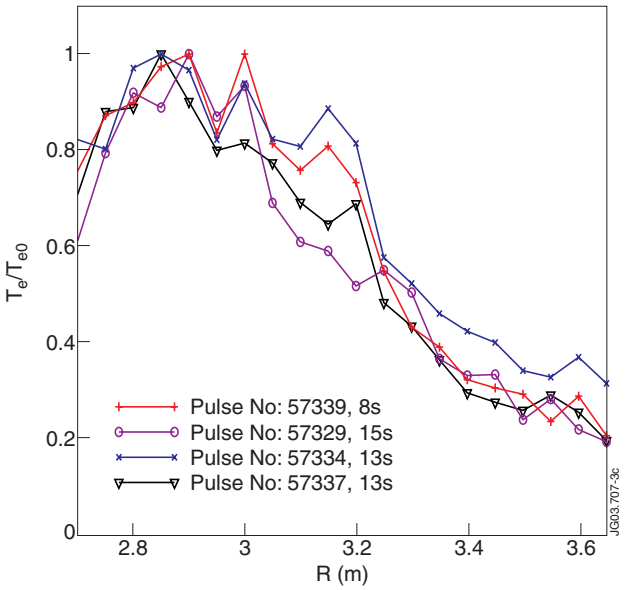

Figure 3: Electron temperature profiles from LIDAR Thomson scattering corresponding to times in fig.2, averaged over 0.8s. Error bars on individual measurements are some 20%. The magnetic axis is at R≅ 2.95m.

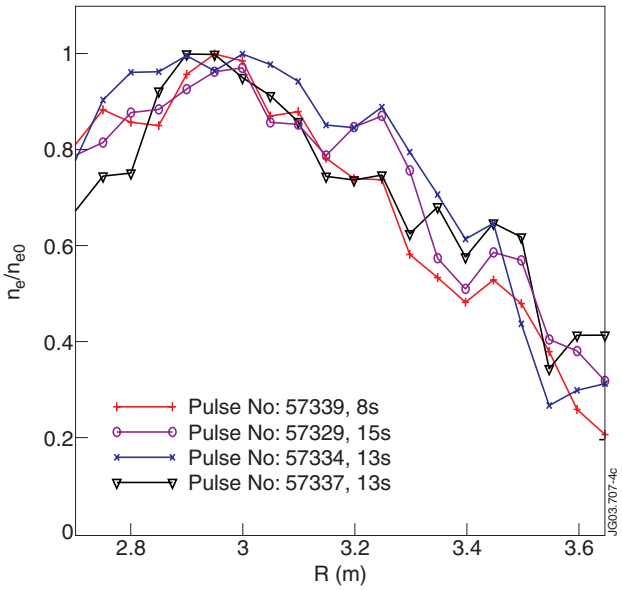

Figure 4: Electron density profiles from LIDAR Thomson scattering corresponding to times in fig.2, averaged over 0.8s. Error bars on individual measurements are some 20%.

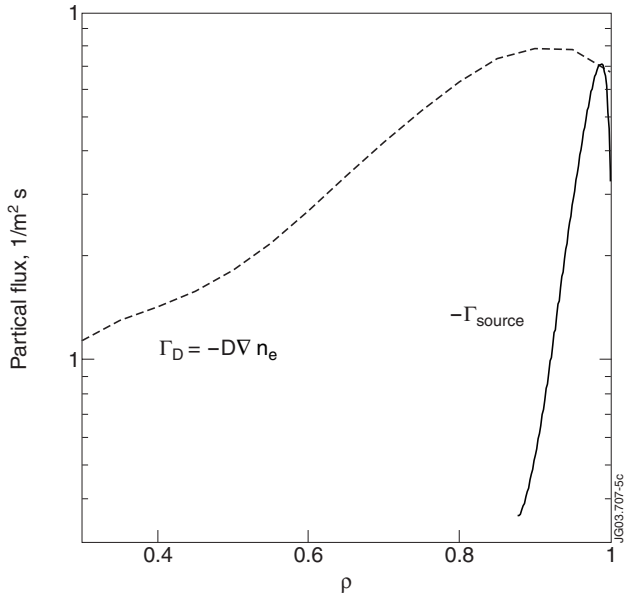

Figure 5: Comparison of the radial profiles of the particle source term (-) and of the estimated diffusive particle flux (--), assuming $D=1m^2/s\ (r/a)^2$.

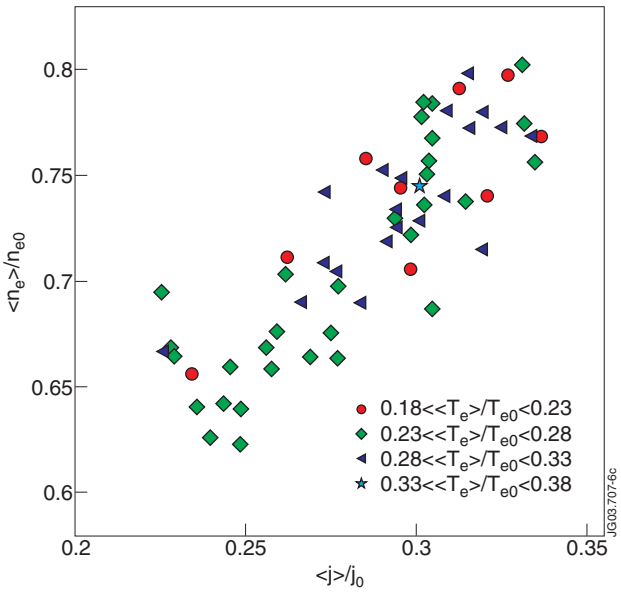

Figure 6: Dependence of density peaking on the peaking of the current profile at constant q_{95} in normal shear discharges. Symbols refer to clesses of electron temperature profile peaking parameter.

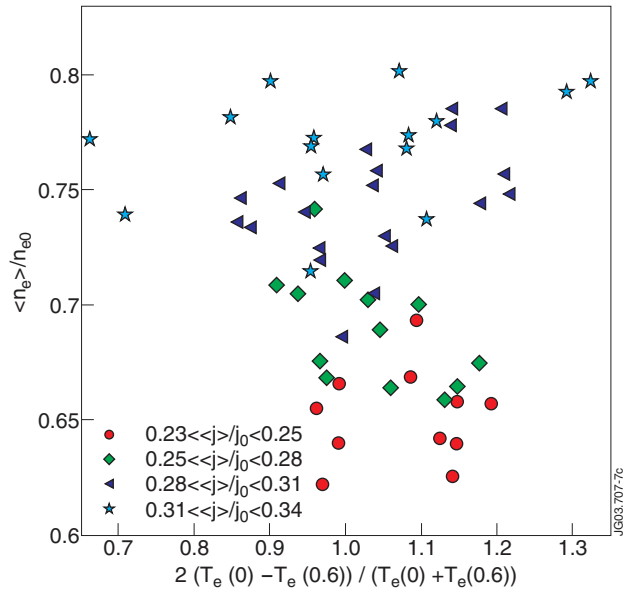

Figure 7: Density peaking versus average electron temperature gradient from ECE in the plasma core region. Symbols refer to classes of current profile peaking.

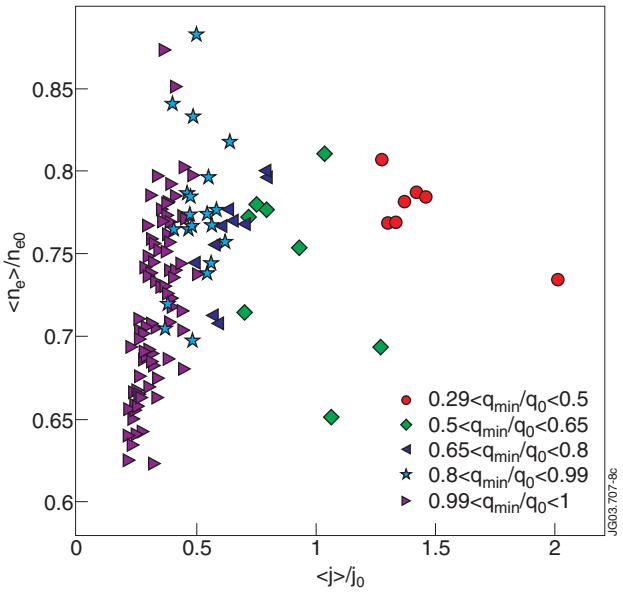

Figure 8: Electron density peaking versus current density peaking (normal and reversed shear)

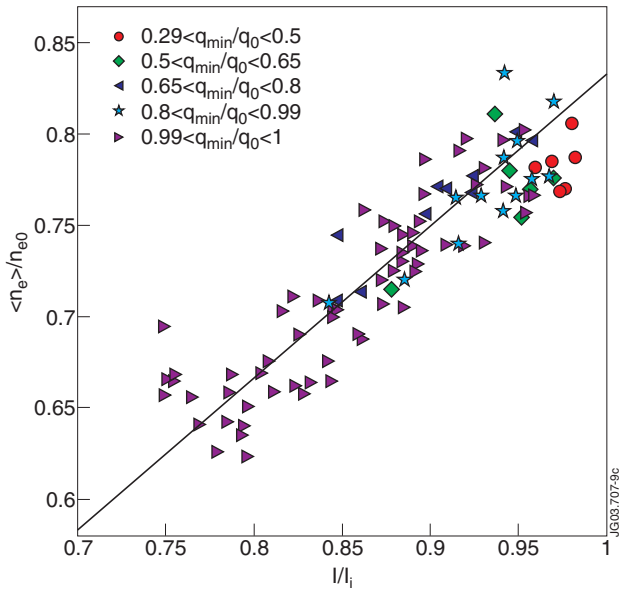

Figure 9: Dependence of density peaking on internal inductance. Symbols refer to reversal parameter.

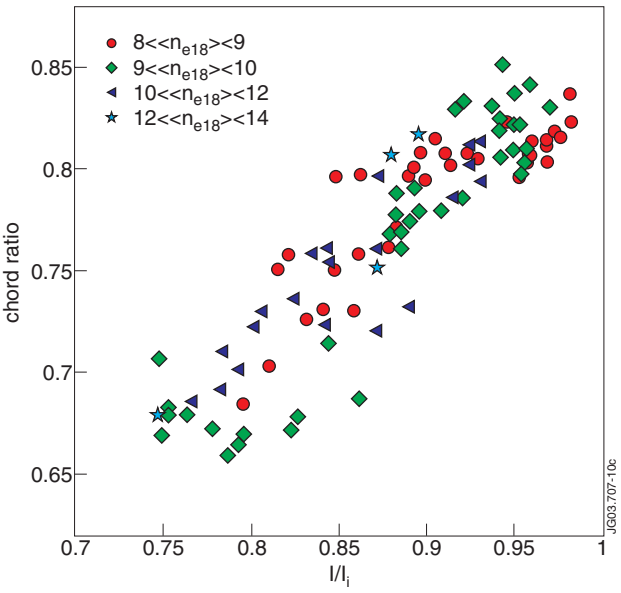

Figure 10: Ratio of chord #5 (off-axis) and chord #8 (on-axis) line density measurement versus $1/l_i$.

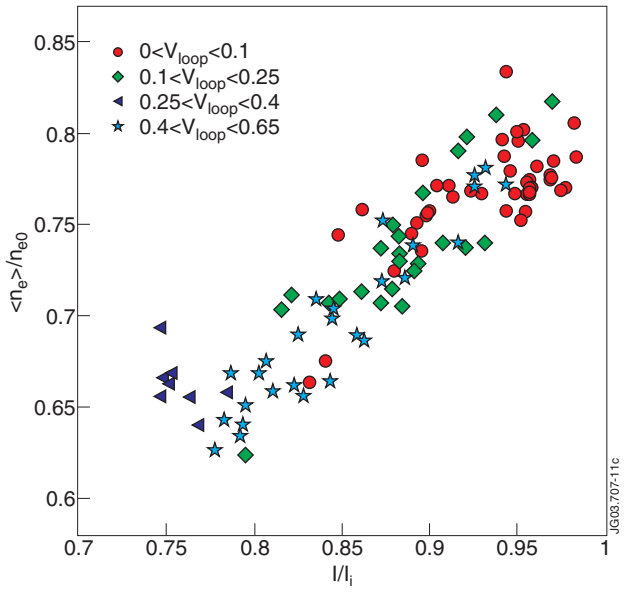

Figure 11: Dependence of density peaking on internal inductance, resolved into classes of loop voltage.

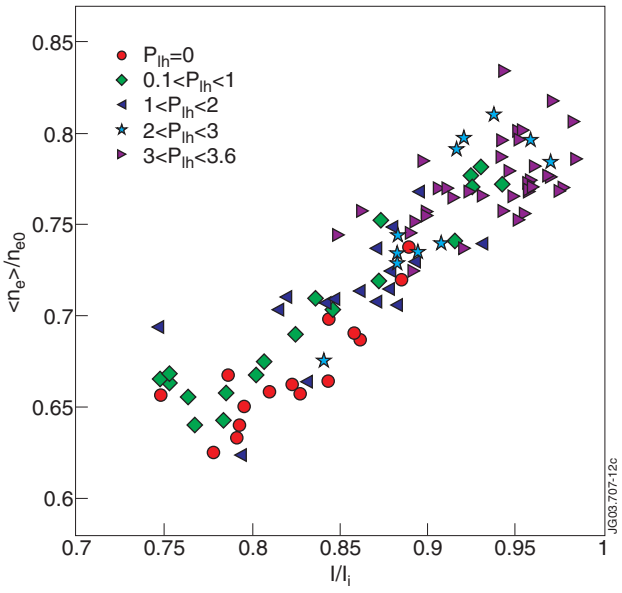

Figure 12: Dependence of density peaking on internal inductance, resolved into classes of LHCD power (MW).

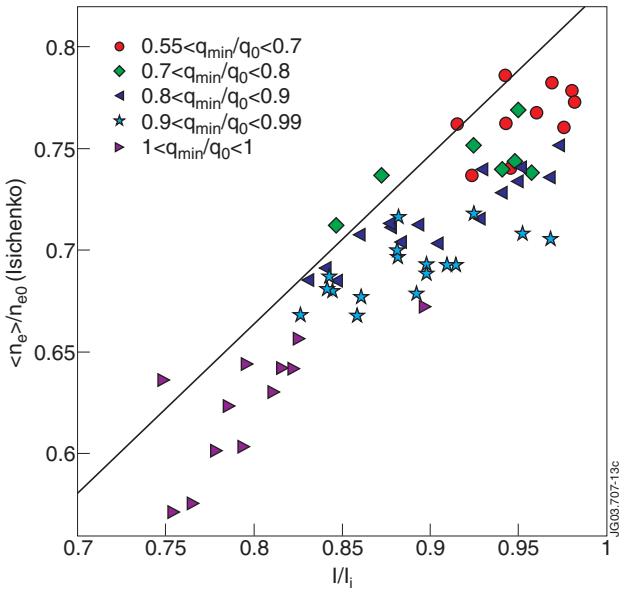

Figure 13: Scaling with internal inductance of the density peaking factor of Isichenko's canonical profiles. Symbols refer to the reversal parameter. Safety factor profiles were taken from polarimetr-constrained equilibrium reconstructions. The line represents the average trend of the experimental data.

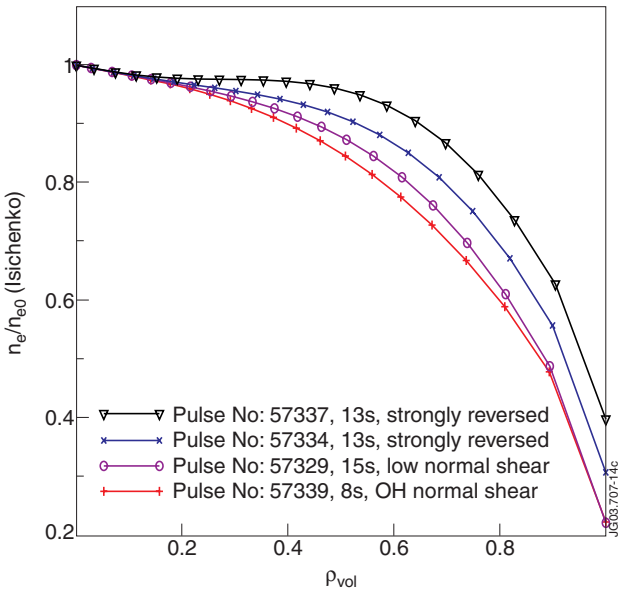

Figure 14: Examples of 'canonical' density profiles following Isichenko, modelled using the safety factor profiles in fig.2.

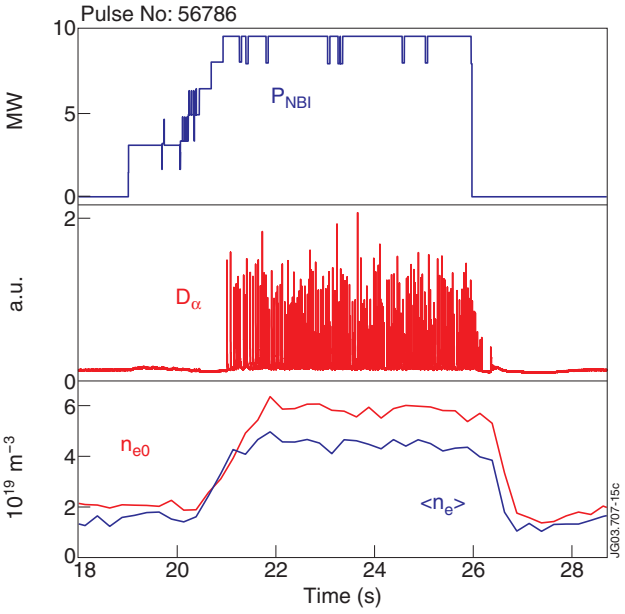

Figure 15: Evolution of density peaking in an NBI heated H-mode in JET Top: NBI heating power waveform Middle:Deuterium Balmer-alpha light emission from plasma edge Bottom: Axial and volume average electron densities

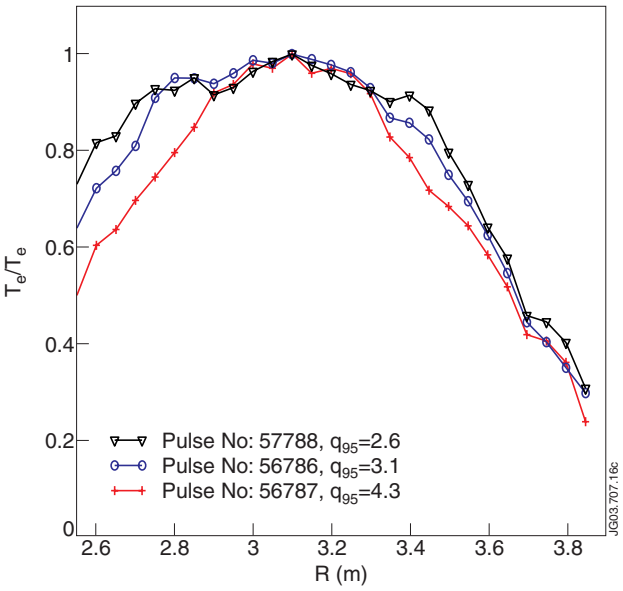

Figure 16: Electron temperature profiles in three ELMy H-mode plasmas with different edge safety factors.

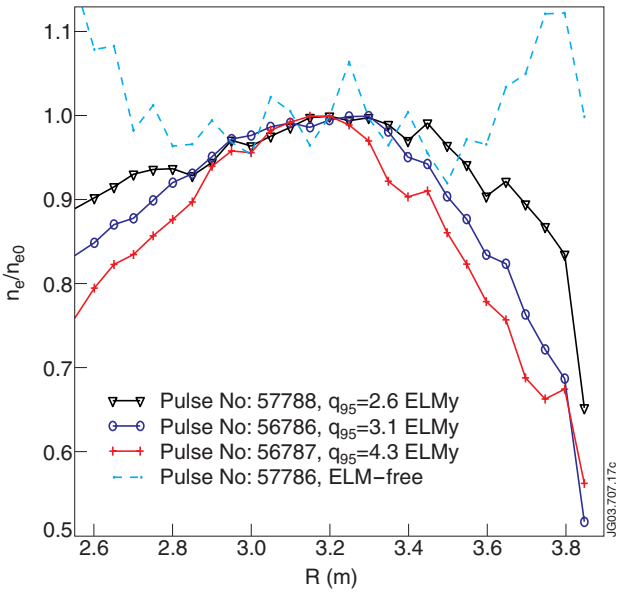

Figure 17: Electron density profiles in three ELMy H-mode plasmas with different edge safety factors (solid lines). Electron density profile (broken line) during the transient ELM-free phase following the L-H transition in Pulse No: 57786.